

UV Volumes for Real-time Rendering of Editable Free-view Human Performance

YUE CHEN*, Xi'an Jiaotong University, China

XUAN WANG*, Tencent AI Lab, China

QI ZHANG, Tencent AI Lab, China

XIAOYU LI, Tencent AI Lab, China

XINGYU CHEN, Xi'an Jiaotong University, China

YU GUO, Xi'an Jiaotong University, China

JUE WANG, Tencent AI Lab, China

FEI WANG, Xi'an Jiaotong University, China

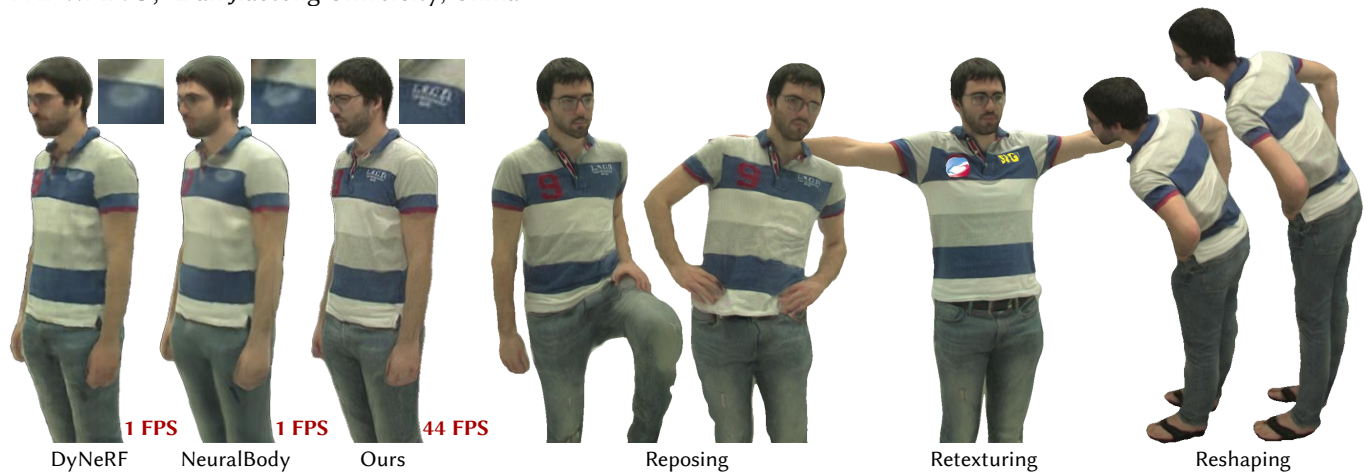


Fig. 1. Novel view synthesis, reposing, retexturing, and reshaping results of proposed UV volume. Compared with baseline methods, our method supports real-time rendering and preserves more sharp image details.

Neural volume rendering has been proven to be a promising method for efficient and photo-realistic rendering of a human performer in free-view, a critical task in many immersive VR/AR applications. However, existing approaches are severely limited by their high computational cost in the rendering process. To solve this problem, we propose the *UV Volumes*, an approach that can render an editable free-view video of a human performer in real-time. It is achieved by removing the high-frequency (i.e., non-smooth) human textures from the 3D volume and encoding them into a 2D neural texture stack (NTS). The smooth UV volume allows us to employ a much smaller and shallower structure for 3D CNN and MLP, to obtain the density and texture coordinates without losing image details. Meanwhile, the NTS

only needs to be queried once for each pixel in the UV image to retrieve its RGB value. For editability, the 3D CNN and MLP decoder can easily fit the function that maps the input structured-and-posed latent codes to the relatively smooth densities and texture coordinates. It gives our model a better generalization ability to handle novel poses and shapes. Furthermore, the use of NTS enables new applications, e.g., retexturing. Extensive experiments on CMU Panoptic, ZJU Mocap, and H36M datasets show that our model can render 900×500 images in 40 fps on average with comparable photorealism to state-of-the-art methods. The project and supplementary materials are available at <https://fanegg.github.io/UV-Volumes>.

CCS Concepts: • **Computing methodologies** → **Rendering**.

Additional Key Words and Phrases: Neural Rendering

ACM Reference Format:

Yue Chen, Xuan Wang, Qi Zhang, Xiaoyu Li, Xingyu Chen, Yu Guo, Jue Wang, and Fei Wang. 2018. UV Volumes for Real-time Rendering of Editable Free-view Human Performance. *ACM Trans. Graph.* 37, 4, Article 111 (August 2018), 8 pages. <https://doi.org/XXXXXXX.XXXXXXX>

1 INTRODUCTION

Synthesizing a free-view video of a human performer in motion is a long-standing problem in computer graphics. Early approaches [Collet et al. 2015a] rely on obtaining an accurate 3D mesh sequence through multi-view stereo and the corresponding texture images.

*Both authors contributed equally to this research.

Authors' addresses: Yue Chen, Xi'an Jiaotong University, China; Xuan Wang, Tencent AI Lab, China; Qi Zhang, Tencent AI Lab, China; Xiaoyu Li, Tencent AI Lab, China; Xingyu Chen, Xi'an Jiaotong University, China; Yu Guo, Xi'an Jiaotong University, China; Jue Wang, Tencent AI Lab, China; Fei Wang, Xi'an Jiaotong University, China.

Permission to make digital or hard copies of all or part of this work for personal or classroom use is granted without fee provided that copies are not made or distributed for profit or commercial advantage and that copies bear this notice and the full citation on the first page. Copyrights for components of this work owned by others than ACM must be honored. Abstracting with credit is permitted. To copy otherwise, or republish, to post on servers or to redistribute to lists, requires prior specific permission and/or a fee. Request permissions from permissions@acm.org.

© 2018 Association for Computing Machinery.

0730-0301/2018/8-ART111 \$15.00

<https://doi.org/XXXXXXX.XXXXXXX>

However, the computed 3D mesh often fails to depict the complex geometry structure, resulting in damaged photorealism. In recent years, methods (e.g., NeRF [Mildenhall et al. 2020]) that make use of volumetric representation and differentiable ray casting have shown promising results for novel view synthesis. These techniques have been further extended to tackle dynamic scenes.

Nonetheless, NeRF and its variants require a large number of queries against a deep MLP. Such time-consuming computation prevents them from being applied to applications that require high rendering efficiency. In the case of static NeRF, a few methods [Garbin et al. 2021; Reiser et al. 2021; Yu et al. 2021b] have already achieved real-time performance. However, for dynamic NeRF, solutions for real-time rendering of volumetric free-view video are still lacking.

In this paper, we present a novel framework, *UV Volumes*, which can produce an editable free-view video of a human performer in motion and render it in real-time. Specifically, we utilize the availability of a pre-defined UV-unwrapping (e.g., SMPL or dense pose) of the human body to tackle the geometry (with texture coordinates) and textures in two branches. We employ a sparse 3D CNN to transform the voxelized and structured latent codes anchored with a posed SMPL model to a 3D feature volume, in which only smooth and view-independent densities and UV coordinates are encoded. For rendering efficiency, we use a shallow MLP to decode the density and integrate the feature into the image plane by volume rendering. Each feature in the image plane is then converted to the UV coordinates individually. Accordingly, we utilize the yielded UV coordinates to query the RGB value from a pose-dependent neural texture stack (NTS). This process greatly reduces the number of queries against MLPs and enables real-time rendering.

It is worth noting that the network modules in the proposed framework only need to approximate relatively "smooth" functions. That is because both density and UV coordinate can be regarded as low-frequency signals, and the detailed appearance encoded in the NTS is spatially aligned across different poses. This increases the generalization of such modules and supports various editing operations.

We perform extensive experiments on three widely-used datasets: CMU Panoptic, ZJU Mocap, and H36M datasets. The results show that the proposed approach can effectively generate editable free-view video from both dense and sparse views. The produced free-view video can be rendered in real-time with comparable photorealism to the state-of-the-art methods that have much higher computational costs. In summary, our major contributions are:

- A novel system for rendering editable human performance video in free-view and real-time.
- UV Volumes, a method that can accelerate the rendering process while preserving the high-frequency details.
- Extended editing applications enabled by this framework, such as reposing, retexturing, and reshaping.

2 RELATED WORK

Novel View Synthesis for Static Scenes. Novel view synthesis for static scenes is a well-explored problem. Early image-based rendering approaches [Davis et al. 2012; Gortler et al. 1996; Levoy and Hanrahan 1996] utilize densely sampled images to obtain novel

views with light fields instead of explicit or accurate geometry estimation. The learning-based methods [Flynn et al. 2019; Kalantari et al. 2016; Mildenhall et al. 2019; Srinivasan et al. 2019] apply neural networks to reuse input pixels from observed viewpoints. In recent years, dramatic improvements have been achieved by neural volume rendering techniques. For instance, NeRF [Mildenhall et al. 2020] represents a static scene using a deep MLP, mapping 3D spatial locations and 2D viewing directions to volumetric density and radiance. However, rendering high-resolution scenes via NeRF is time-consuming since it requires millions of queries to obtain the density and radiance. Subsequent works [Garbin et al. 2021; Reiser et al. 2021; Yu et al. 2021a,b] attempt to accelerate the inference of vanilla NeRF in various ways, some of which achieve the real-time rendering performance, but only for static scenes.

Free-View Video Synthesis. Early methods [Collet et al. 2015b; Mustafa et al. 2016] rely on accurate 3D reconstruction and texture rendering captured by dome-based multi-camera systems to synthesize novel views of a dynamic scene. Recently, various neural representations are employed in differentiable rendering to depict dynamic scenes, such as the voxels [Lombardi et al. 2019], point clouds [Wu et al. 2020], textured meshes [Thies et al. 2019], and implicit functions [Li et al. 2021b; Liu et al. 2020; Park et al. 2021a,b; Pumarola et al. 2021]. Particularly, DyNeRF [Li et al. 2021b] directly takes the latent code as the condition for time-varying scenes. Other deformation-based NeRF variants [Li et al. 2021a; Park et al. 2021a,b; Pumarola et al. 2021; Tretschk et al. 2021] take as input the monocular video, as a result, they fail to synthesize the free-view spatio-temporal visual effects. Besides, they also suffer from the high computational cost in inference and the lack of editing abilities. A hybrid scene representation is used for efficiency in a very recent approach [Lombardi et al. 2021], but a non-editable model still.

Editable Free-View Videos. There exist previous work that focus on the problem of producing editable free-view video or animatable avatars. ST-NeRF [Zhang et al. 2021] exploits the layered neural representation in order to move, rotate and resize individual objects in free-view videos. Some other approaches rely on the parametric human body model to build an animatable NeRF. Neural Actor [Liu et al. 2021] takes the texture map as latent variables. Unfortunately, the ground-truth texture map usually can not be obtained without high-fidelity 3D reconstruction. In contrast, without using any high-fidelity 3D reconstructions, our approach can produce editable (including reposing, reshaping and retexturing) free-view videos in real-time from both dense and sparse views.

3 METHOD

Given multi-view videos of a performer, our model generates an editable free-view video that supports real-time rendering. We use the availability of an off-the-shelf SMPL model and the pre-defined UV unwrap in Densepose [Güler et al. 2018] to introduce proper priors into our framework. In this section, we describe the details of our framework, which is as shown in Fig. 2. The two main branches in our framework are presented in turn. One is to generate the UV volumes (Sec. 3.1), and the other is the generation of NTS (Sec. 3.2). Then we provide the more detailed description of the training process in Sec. 3.3.

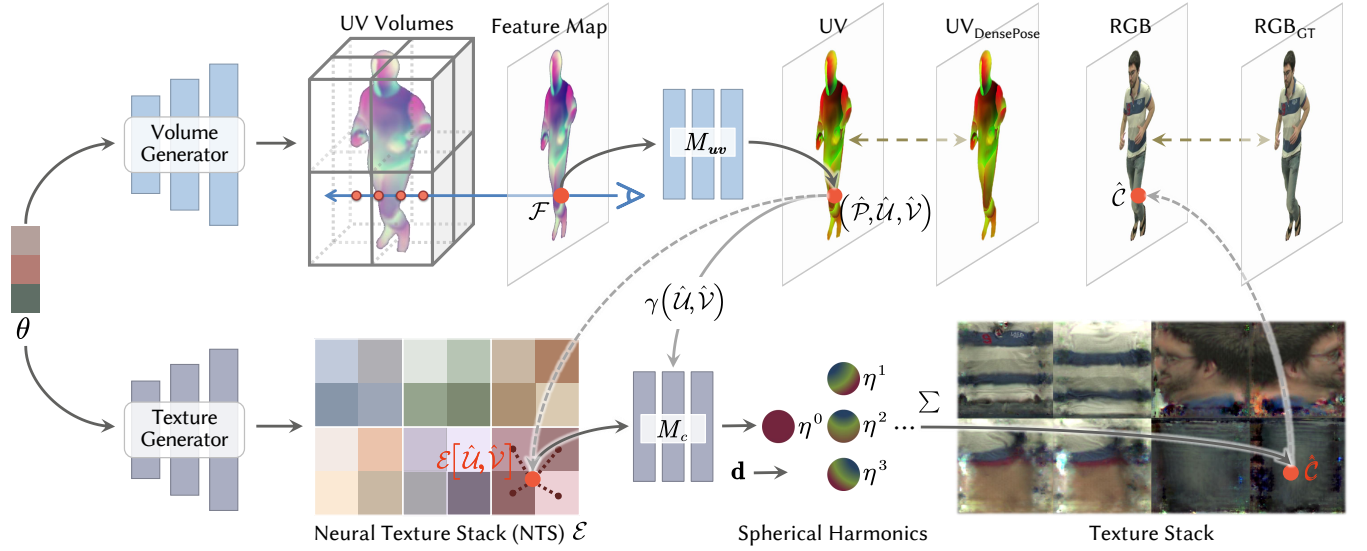


Fig. 2. Overall pipeline of proposed framework. Our model has two main branches: 1) Based on a human pose θ , a volume generator constructs UV volumes involving the feature of UV information. Then a feature map can be rendered via differentiable raymarching and decoded to texture coordinates (UV) pixel-by-pixel. 2) A texture generator produces a pose-dependent NTS encoding the highly-detailed appearance information. The UV coordinates and the texture embedding interpolated by it are passed into an MLP to predict spherical harmonic coefficients η . The final color \hat{C} can be calculated by summing the weighted spherical harmonic bases evaluated at the desired ray direction \mathbf{d} .

3.1 UV Volumes

Neural radiance fields [Mildenhall et al. 2020] have been proven to produce free-viewpoint images with view consistency and high fidelity. Nonetheless, capturing the high-fidelity appearance in a dynamic scene is time-consuming and difficult. To this end, we propose the UV volumes in which only the density and texture coordinate (i.e., UV coordinate) are encoded instead of human appearance. Thanks to the UV unwrap defined in Densepose, we can use the UV coordinate to query the corresponding RGB values from the 2D NTS when the UV image is rendered by ray casting.

We utilize the volume generator to construct UV volumes. First, the time-invariant latent codes anchored to a posed SMPL model are voxelized and taken as the input. Then we use the 3D sparse CNN to encode the voxelized latent codes to a 3D feature volume named the UV volumes, which contains UV information.

Given a sample image \mathcal{I} of multi-view videos, we provide a posed SMPL parameterized by human pose θ and a set of latent codes \mathbf{z} anchored on its vertices and then query the feature vector $f(\mathbf{x}, \mathbf{z}, \theta)$ at point \mathbf{x} from the generated UV volumes. The feature vector is fed into a shallow MLP M_σ to predict the volume density:

$$\sigma(\mathbf{x}) = M_\sigma(f(\mathbf{x}, \mathbf{z}, \theta)). \quad (1)$$

We then apply the volume rendering [Kajiya and Von Herzen 1984] technique to render the UV feature volume into a 2D feature map. We sample N_i points $\{\mathbf{x}_i\}_{i=1}^{N_i}$ along the camera ray \mathbf{r} between near and far bounds based on the posed SMPL model in 3D space. The feature at the pixel can be calculated as:

$$\begin{aligned} \mathcal{F}(\mathbf{r}) &= \sum_{i=1}^{N_i} T_i (1 - \exp(-\sigma(\mathbf{x}_i) \delta_i)) f(\mathbf{x}_i, \mathbf{z}, \theta), \\ T_i &= \exp\left(-\sum_{j=1}^{i-1} \sigma(\mathbf{x}_j) \delta_j\right), \end{aligned} \quad (2)$$

where $\delta_i = \|\mathbf{x}_{i+1} - \mathbf{x}_i\|_2$ is the distance between adjacent sampled points. An MLP M_{uv} is used to individually decode all the pixels in the yielded view-invariant feature image to their corresponding texture coordinates to generate the UV image. In specific, the texture coordinates can be represented as:

$$(\hat{\mathcal{P}}(\mathbf{r}), \hat{\mathcal{U}}(\mathbf{r}), \hat{\mathcal{V}}(\mathbf{r})) = M_{uv}(\mathcal{F}(\mathbf{r})), \quad (3)$$

where $\hat{\mathcal{P}}$ and $\hat{\mathcal{U}}, \hat{\mathcal{V}}$ respectively are the corresponding part assignments and UV coordinates.

3.2 Neural Texture Stack

Given the generated UV image, we employ the continuous texture stack encoded in the implicit neural representation to recover the color image. To model the dynamic details in texture, we take as input the pose parameter θ and use a CNN texture generator G to produce the pose-dependent NTS:

$$\mathcal{E}_k = G(\theta, \mathbf{k}), \quad (4)$$

where we subdivide the body surface into $N_k = 24$ parts, and \mathbf{k} is a one-hot vector representing the k -th body part. At a foreground pixel, the part assignments $\hat{\mathcal{P}}$ predicted from UV volumes (referred in Equation (3)) can be interpreted as the probability of the pixel to belong to the k -th body part, which is defined as $\sum_{k=1}^{N_k} \hat{\mathcal{P}}_k(\mathbf{r}) = 1$. The coordinate maps $\hat{\mathcal{U}}_k$ and $\hat{\mathcal{V}}_k$ correspond to the pixel coordinates on the k -th body part. We sample the texture embeddings at non-integer locations $(\hat{\mathcal{U}}_k(\mathbf{r}), \hat{\mathcal{V}}_k(\mathbf{r}))$ in a piecewise-differentiable manner using bilinear interpolation [Jaderberg et al. 2015]:

$$\mathbf{e}_k(\mathbf{r}) = \mathcal{E}_k[\hat{\mathcal{U}}_k(\mathbf{r}), \hat{\mathcal{V}}_k(\mathbf{r})]. \quad (5)$$

To model high-frequency color of human performances, we apply the positional encoding $\gamma(\cdot)$ [Rahaman et al. 2019] to UV coordinates, and pass the encoded UV map with the sampled texture embedding

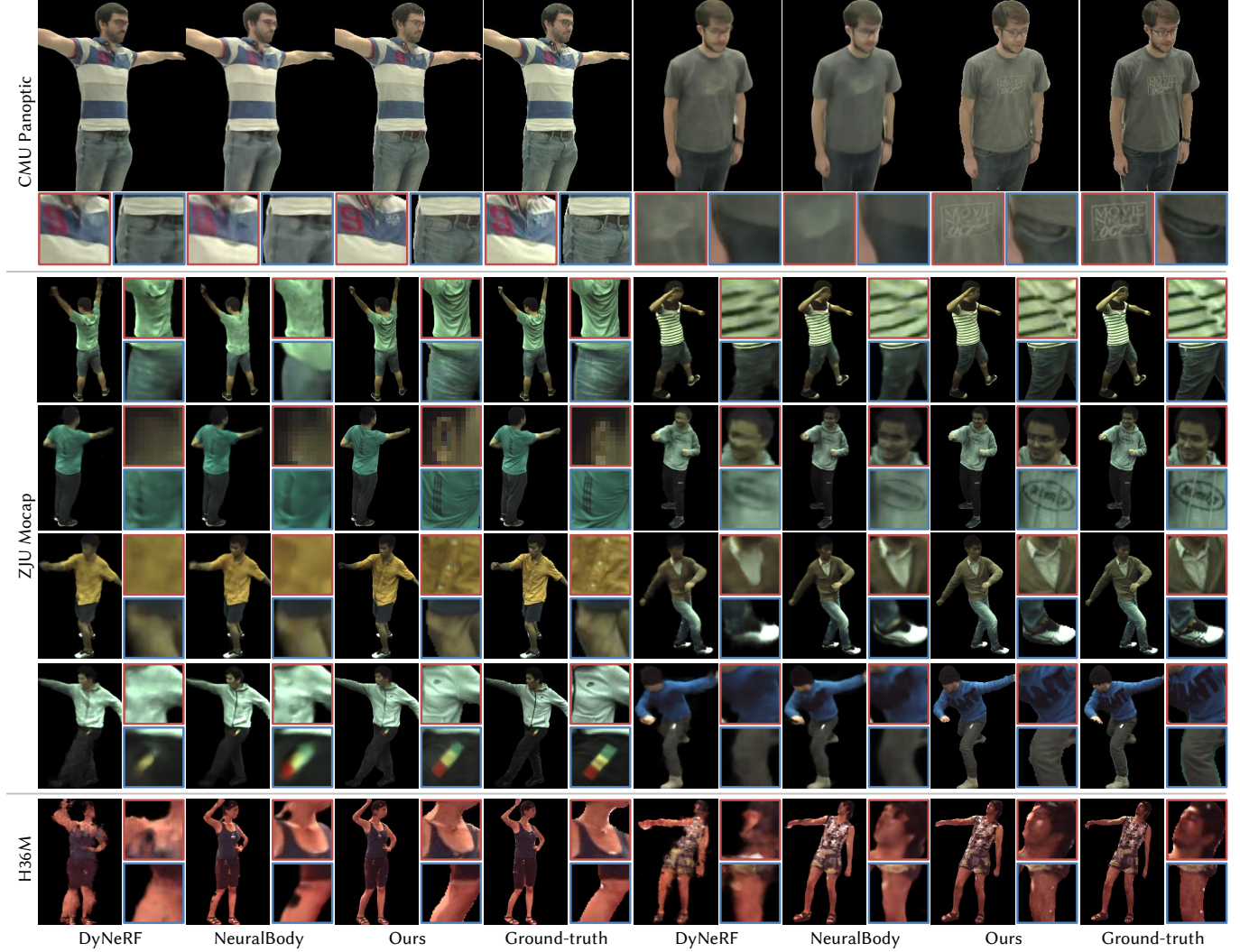


Fig. 3. Qualitative results of novel view synthesis on CMU Panoptic, ZJU Mocap, and H36M datasets. It is illustrated that our method produces the high-fidelity novel synthesis results. All the baseline methods suffer from blurry textures, especially in letters and wrinkles. In the challenging experiment on H36M dataset with sparse training views, DyNeRF fails to generate plausible results.

into an MLP M_c to decode the spherical harmonic coefficients η for each color channel:

$$\left(\hat{\eta}_k^0(\mathbf{r}), \hat{\eta}_k^1(\mathbf{r}), \dots, \hat{\eta}_k^n(\mathbf{r})\right) = M_c\left(\gamma(\hat{\mathcal{U}}_k(\mathbf{r}), \hat{\mathcal{V}}_k(\mathbf{r})), \mathbf{e}_k(\mathbf{r}), \mathbf{k}\right), \quad (6)$$

where spherical harmonics $(\eta^0, \eta^1, \dots, \eta^n)$ form an orthogonal basis for functions defined over the sphere, with zero degree harmonics η^0 encoding diffuse color and higher degree harmonics encoding specular effects. The view-dependent color $\hat{C}_k(\mathbf{r})$ of camera ray \mathbf{r} may be determined by querying the specular spherical functions SH at the desired viewing direction \mathbf{d} :

$$\hat{C}_k(\mathbf{r}) = S\left(\frac{\hat{\eta}_k^0(\mathbf{r})}{2}\sqrt{\frac{1}{\pi}} + \sum_{m=1}^n SH^m(\hat{\eta}_k^m(\mathbf{r}), \mathbf{d})\right), \quad (7)$$

where S is the sigmoid function for normalizing the colors. Following that, the color $\hat{C}(\mathbf{r})$ at each pixel is reconstructed via a weighted combination of decoded colors at N_k body parts, where the weights

are prescribed by part assignments $\hat{\mathcal{P}}_k$:

$$\hat{C}(\mathbf{r}) = \sum_{k=1}^{N_k} \hat{\mathcal{P}}_k(\mathbf{r}) \hat{C}_k(\mathbf{r}). \quad (8)$$

3.3 Training

Collecting the results of all rays $\{\hat{C}(\mathbf{r})\}^{H \times W}$, we denote the full rendered image as $\hat{I} \in \mathbb{R}^{H \times W \times 3}$. To learn the parameters of our model, we optimize the L2 loss between the rendered \hat{I} and observed images I :

$$\mathcal{L}_{\text{rgb}} = \left\| \hat{I} - I \right\|_2^2. \quad (9)$$

In contrast to [Mildenhall et al. 2020; Peng et al. 2021], we can render an entire image requiring a single pass through our model.



Fig. 4. Qualitative results of novel pose synthesis on CMU Panoptic, ZJU Mocap, and H36M dataset. We compare our method against NeuralBody on synthesizing the novel poses. Benefiting from the UV volumes and NTS that give our models better generalization ability, our method performs better on novel poses, especially for preserving sharp image details.

Thus, we also compare the rendered images against the ground-truth using perceptual loss [Gatys et al. 2016; Johnson et al. 2016; Ulyanov et al. 2016], which extracts feature maps by pretrained fixed VGG network $\psi(\cdot)$ [Simonyan and Zisserman 2014] from both images and minimizes the L1-norm between them:

$$\mathcal{L}_{\text{vgg}} = \left\| \psi(\hat{I}) - \psi(I) \right\|_1. \quad (10)$$

To warm-start the UV volumes and regularize its solution space, we leverage the pre-trained DensePose model. In particular, we perform the DensePose on the training data to produce the Densepose UV image as pseudo supervision, to regularize the UV volumes under

semantic loss \mathcal{L}_p and UV-metric loss \mathcal{L}_{uv} between the DensePose outputs and our UV predictions:

$$\begin{aligned} \mathcal{L}_p &= \sum_{k=1}^{N_k} \mathcal{P}_k \log(\hat{\mathcal{P}}_k), \\ \mathcal{L}_{\text{uv}} &= \sum_{k=1}^{N_k} \mathcal{P}_k \left(\left\| \hat{\mathcal{U}}_k - \mathcal{U}_k \right\|_2^2 + \left\| \hat{\mathcal{V}}_k - \mathcal{V}_k \right\|_2^2 \right), \end{aligned} \quad (11)$$

where N_k is the number of body parts, and \mathcal{P}_k and $\hat{\mathcal{P}}_k$ are respectively the multi-class semantic probability at the k -th part of DensePose outputs and UV volumes predictions. Similarly, $\mathcal{U}_k, \mathcal{V}_k$ and

Datasets		PSNR↑			SSIM↑			LPIPS↓			FPS↑		
		DyNeRF	NeuralBody	Ours	DyNeRF	NeuralBody	Ours	DyNeRF	NeuralBody	Ours	DyNeRF	NeuralBody	Ours
CMU 26 views	Blue	30.04	29.78	30.38	0.968	0.962	0.966	0.088	0.099	0.036	1.01	0.76	44.76
	Gray	26.11	28.94	27.45	0.937	0.952	0.947	0.137	0.140	0.066	0.90	0.66	36.02
	Plaid	25.78	27.20	27.30	0.917	0.930	0.922	0.180	0.159	0.071	1.23	1.12	39.84
ZJU 20 views	313	31.95	32.22	31.12	0.977	0.979	0.975	0.037	0.036	0.038	2.24	1.23	45.07
	377	27.27	27.92	26.28	0.938	0.948	0.933	0.101	0.085	0.079	2.85	2.05	37.15
	386	29.78	29.74	28.09	0.938	0.936	0.919	0.102	0.101	0.075	2.51	1.97	35.55
ZJU 4 views	313	20.11	30.14	29.56	0.886	0.972	0.967	0.189	0.046	0.045	3.58	2.59	38.83
	377	21.19	28.59	26.17	0.845	0.952	0.938	0.214	0.074	0.079	2.83	1.50	37.43
	386	28.24	30.07	27.94	0.920	0.938	0.918	0.115	0.086	0.077	2.65	1.76	35.68
H36M 3 views	s9p	21.52	25.11	26.19	0.824	0.912	0.916	0.242	0.136	0.084	1.06	2.19	40.00
	s11p	21.27	24.39	25.82	0.828	0.899	0.911	0.313	0.193	0.111	1.18	1.02	33.41
	s1p	18.91	23.24	23.98	0.781	0.909	0.911	0.332	0.149	0.093	1.38	0.97	41.43

Table 1. Quantitative results of novel view synthesis. We achieve competitive PSNR and SSIM while outperforming the others on LPIPS and FPS.

Methods	CMU 26 Views			ZJU 20 Views			H36M 3 Views		
	PSNR↑	SSIM↑	LPIPS↓	PSNR↑	SSIM↑	LPIPS↓	PSNR↑	SSIM↑	LPIPS↓
NeuralBody	25.94	0.918	0.146	24.51	0.918	0.120	24.67	0.872	0.185
Ours	26.20	0.927	0.073	23.69	0.910	0.104	24.32	0.863	0.141

Table 2. Quantitative results of novel pose synthesis. We achieves competitive PSNR and SSIM while outperforming NeuralBody on LPIPS.

$\hat{\mathcal{U}}_k, \hat{\mathcal{V}}_k$ are the DensePose and UV volumes predicted UV coordinates at the k -th part. \mathcal{L}_p is chosen as a multi-class cross-entropy loss to encourage rendered part labels to be consistent with provided DensePose labels, and \mathcal{L}_{uv} promotes to generate inter-frame consistent UV coordinates.

Given the binary human mask \mathcal{S} for the observed image \mathcal{I} , we propose a silhouette loss to facilitate UV volumes modeling a more fine-grained geometry:

$$\mathcal{L}_s = \sum_{\mathbf{r} \in \mathcal{R}} (\mathcal{S}(\mathbf{r})(1 - T(\mathbf{r})) + (1 - \mathcal{S}(\mathbf{r}))T(\mathbf{r})), \quad (12)$$

$$\text{where } T(\mathbf{r}) = \exp\left(-\sum_{j=1}^{N_f-1} \sigma(\mathbf{x}_j) \delta_j\right),$$

where $T(\mathbf{r})$ is accumulated transmittance. The value of mask $\mathcal{S}(\mathbf{r})$ in the foreground is zero, and the background is one.

We combine the aforementioned losses and jointly train our model to optimize the full objective:

$$\mathcal{L} = \mathcal{L}_{rgb} + \lambda_{vgg} \mathcal{L}_{vgg} + \lambda_p \mathcal{L}_p + \lambda_{uv} \mathcal{L}_{uv} + \lambda_s \mathcal{L}_s. \quad (13)$$

4 EXPERIMENTS

To demonstrate the effectiveness and efficiency of our method, we perform extensive experiments. We report quantitative results using four standard metrics: PSNR, SSIM, LPIPS, and FPS. And the qualitative experiments illustrate our method produces photo-realistic images in different tasks, e.g., novel view synthesis, reposing, reshaping, and retexturing.

Dataset. We perform experiments on several types of datasets which consist of calibrated and synchronized multi-view videos. We use 26 training views for experiments on CMU Panoptic dataset [Joo et al. 2017]. For the ZJU-Mocap dataset [Fang et al. 2021; Peng et al. 2021], we consider two regimes: training on 20 or 4 views. Last is the H36M dataset [Ionescu et al. 2013], the most challenging one

where only three cameras are available for training. The evaluation is done on the hold-out cameras (novel views) or hold-out segments of the sequence (novel poses).

Baselines. To validate our method, we compare against two state-of-the-art free-view video synthesis techniques: 1) DyNeRF [Li et al. 2021b], which takes time-varying latent codes as the conditions for dynamic scenes; and 2) NeuralBody [Peng et al. 2021], which takes as input the posed human model with structured time-invariant latent codes and generate a pose-conditioned neural radiance field.

Novel View Synthesis. For comparison, we synthesize images of training poses in hold-out test views. Table 1 shows the comparison of our method against baselines, which demonstrates that our method performs best LPIPS and FPS among all methods. Specifically, we achieve rendering the free-view videos of human performances in 40 FPS with the help of UV volumes.

Figure 1 and Figure 3 present the qualitative comparison of our method with baselines. Both NeuralBody and DyNeRF fail to preserve the sharp image details. As shown in the first person of Figure 3, their rendering miss letters on the shirt and belt on the pants. In contrast, our method can accurately capture the high-frequency details benefiting from our NTS model.

Furthermore, DyNeRF fails to render plausible results with sparse training views because taking time-varying latent codes as the conditions is hard to reuse information among frames.

Pose Editing. We perform reposing on the human performer with novel motions. As DyNeRF is not designed for editing tasks, we only compare our method against NeuralBody. As shown in Table 2, quantitative results demonstrate our method achieves competitive PSNR and SSIM while outperforming NeuralBody on LPIPS.

The qualitative results are shown in Figure 1 and Figure 4. NeuralBody gives blurry and distorted rendering results for complex novel human poses. In contrast, synthesized images of our method achieve better visual quality with reasonable high-definition dynamic textures. The results indicate that using smooth UV volumes in 3D and encoding texture in 2D has better controllability on the novel pose synthesis than directly modeling a pose-conditioned neural radiance field.

Shape Editing. We demonstrate that our approach can edit the shape of reconstructed human performance by changing shape parameters of the SMPL model. We report the qualitative results on the Figure 1 and Figure 5. NeuralBody fails to infer the reasonable

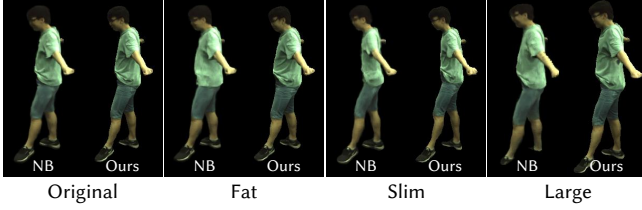


Fig. 5. Qualitative results of shape editing. By changing the SMPL parameters β , we can conveniently make the human performer fatter, slimmer, or bigger. In each pair of results, the result of NeuralBody is shown on the left, and our result is on the right. Obviously, more details and consistency are preserved in our results in varying shapes.

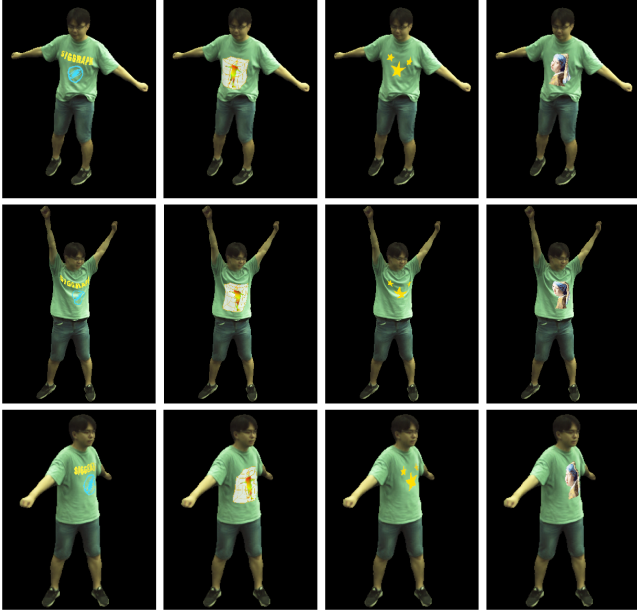


Fig. 6. Qualitative results of texture editing. The presented framework allows us to edit the texture by drawing figures on the NTS conveniently. It is demonstrated that UV Volumes does not only successfully change the texture but also model the dynamics with the novel one.

Task	Ours			w/o UV Loss			w/o VGG Loss		
	PSNR \uparrow	SSIM \uparrow	LPIPS \downarrow	PSNR \uparrow	SSIM \uparrow	LPIPS \downarrow	PSNR \uparrow	SSIM \uparrow	LPIPS \downarrow
Novel Views	31.12	0.975	0.038	31.35	0.972	0.040	30.71	0.972	0.048
Novel Poses	25.32	0.921	0.091	24.98	0.916	0.095	25.27	0.917	0.115

Table 3. Results of models trained with different setting.

Task	60 Frames			300 Frames			600 Frames			1200 Frames		
	PSNR \uparrow	SSIM \uparrow	LPIPS \downarrow	PSNR \uparrow	SSIM \uparrow	LPIPS \downarrow	PSNR \uparrow	SSIM \uparrow	LPIPS \downarrow	PSNR \uparrow	SSIM \uparrow	LPIPS \downarrow
4 Views	29.56	0.967	0.045	29.23	0.963	0.048	29.37	0.964	0.049	28.96	0.961	0.052
20 Views	31.12	0.975	0.038	29.90	0.968	0.046	29.50	0.966	0.048	29.26	0.963	0.053

Table 4. Ablation study of video frames and input views.

changes of the cloth, while our method generalizes well on novel shapes.

Texture Editing. With the learned dense correspondence of UV volumes and neural texture, we can edit the 3D cloth by a user-provided 2D texture, as shown in Figure 6. Visually inspected, the rich texture patterns are well preserved and transferred to correct semantic areas in different poses.

4.1 Ablation Studies

We conduct ablation studies on performer 313 of ZJU dataset. As shown in Table 3, we analyze the effects of different losses for the proposed approach by removing semantic and UV-metric loss (w/o UV Loss) and perceptual loss (w/o VGG loss), respectively. Then we explore the performances of our models trained with different numbers of video frames and input views, as shown in Table 4. Finally, we analyze the time consumption of each module.

Impact of warm-start loss. We present using semantic and UV-metric loss to warm-start the UV volumes and constrain its solution space. To prove the effectiveness of this process, we train an ablation (w/o UV Loss) built upon our full model by eliminating the warm-start loss. It gives higher PSNR when rendering novel views but bad performance in all metrics when rendering novel poses. This comparison indicates that the warm-start loss yields a better generalization of different poses by constraining the consistency of rendered UV coordinates.

Impact of perceptual loss. Thanks to the UV volumes, we can render an entire image by a single pass during training, allowing us to use perceptual loss. Using the same model but training without the perceptual loss (w/o VGG) gives a lower performance in all metrics. This comparison illustrates that perceptual loss can improve the visual quality of synthesized images.

Impact of the number of camera views and video length. In Table 4, we show the results of our models trained with different numbers of camera views and video frames. All the results are evaluated on the rest two views of the first 60 frame video. The results show that although the number of training views improves the performance on novel view synthesis, sparse four views are good enough for our model to reconstruct dynamic human performances. In addition, the ablation study of frame numbers indicates that training on too many frames may decrease the performance as the network cannot fit such a long video, which is also mentioned in NeuralBody [Peng et al. 2021].

Time consumption. We also analyze the time consumption of each module in our framework on ZJU Mocap performer 313. On average, it takes 37.25 milliseconds (ms) to obtain the UV volumes from the input. Then it spends 7.24 ms to decode the volume densities and 3.18 ms to render the volume into a feature map. Next, only 1.96 ms is needed to convert the features to the UV image. At last, it takes about 9.71ms to access the neural texture stack. In summary, we can render in 22 milliseconds per frame (45 FPS) for the task of free-view videos since the UV volumes can be pre-generated. Even on the novel pose synthesis task, our method can reach 59 milliseconds per frame (16 FPS) as well.

5 CONCLUSIONS

We have presented the UV volumes for free-view video synthesis of a human performer. It is the first method to generate the realtime free-view video with editing ability. The key idea is to employ the smooth UV volumes and highly-detailed textures in an implicit neural texture stack. Extensive experiments have demonstrated both the effectiveness and efficiency of our method. In addition to improving efficiency, our approach can also support editing, e.g., reposing, reshaping, or retexturing the human performer in the free-view videos.

REFERENCES

- Alvaro Collet, Ming Chuang, Pat Sweeney, Don Gillett, Dennis Evseev, David Calabrese, Hugues Hoppe, Adam Kirk, and Steve Sullivan. 2015a. High-quality streamable free-viewpoint video. *ACM Transactions on Graphics (ToG)* 34, 4 (2015), 1–13.
- Alvaro Collet, Ming Chuang, Pat Sweeney, Don Gillett, Dennis Evseev, David Calabrese, Hugues Hoppe, Adam Kirk, and Steve Sullivan. 2015b. High-quality streamable free-viewpoint video. *ACM Transactions on Graphics (ToG)* 34, 4 (2015), 1–13.
- Abe Davis, Marc Levoy, and Fredo Durand. 2012. Unstructured light fields. In *Computer Graphics Forum*, Vol. 31. Wiley Online Library, 305–314.
- Qi Fang, Qing Shuai, Junting Dong, Hujun Bao, and Xiaowei Zhou. 2021. Reconstructing 3D Human Pose by Watching Humans in the Mirror. In *CVPR*.
- John Flynn, Michael Broxton, Paul Debevec, Matthew DuVall, Graham Fyfe, Ryan Overbeck, Noah Snaveley, and Richard Tucker. 2019. Deepview: View synthesis with learned gradient descent. In *Proceedings of the IEEE/CVF Conference on Computer Vision and Pattern Recognition*. 2367–2376.
- Stephan J Garbin, Marek Kowalski, Matthew Johnson, Jamie Shotton, and Julien Valentin. 2021. Fastnerf: High-fidelity neural rendering at 200fps. *arXiv preprint arXiv:2103.10380* (2021).
- Leon A Gatys, Alexander S Ecker, and Matthias Bethge. 2016. Image style transfer using convolutional neural networks. In *Proceedings of the IEEE conference on computer vision and pattern recognition*. 2414–2423.
- Steven J Gortler, Radek Grzeszczuk, Richard Szeliski, and Michael F Cohen. 1996. The lumigraph. In *Proceedings of the 23rd annual conference on Computer graphics and interactive techniques*. 43–54.
- Riza Alp Güler, Natalia Neverova, and Iasonas Kokkinos. 2018. Densepose: Dense human pose estimation in the wild. In *Proceedings of the IEEE conference on computer vision and pattern recognition*. 7297–7306.
- Catalin Ionescu, Dragos Papava, Vlad Olaru, and Cristian Sminchisescu. 2013. Human3.6m: Large scale datasets and predictive methods for 3d human sensing in natural environments. *IEEE transactions on pattern analysis and machine intelligence* 36, 7 (2013), 1325–1339.
- Max Jaderberg, Karen Simonyan, Andrew Zisserman, et al. 2015. Spatial transformer networks. *Advances in neural information processing systems* 28 (2015), 2017–2025.
- Justin Johnson, Alexandre Alahi, and Li Fei-Fei. 2016. Perceptual losses for real-time style transfer and super-resolution. In *European conference on computer vision*. Springer, 694–711.
- Hanbyul Joo, Tomas Simon, Xulong Li, Hao Liu, Lei Tan, Lin Gui, Sean Banerjee, Timothy Godisart, Bart Nabbe, Iain Matthews, et al. 2017. Panoptic studio: A massively multiview system for social interaction capture. *IEEE transactions on pattern analysis and machine intelligence* 41, 1 (2017), 190–204.
- James T Kajiya and Brian P Von Herzen. 1984. Ray tracing volume densities. *ACM SIGGRAPH computer graphics* 18, 3 (1984), 165–174.
- Nima Khademi Kalantari, Ting-Chun Wang, and Ravi Ramamoorthi. 2016. Learning-based view synthesis for light field cameras. *ACM Transactions on Graphics (TOG)* 35, 6 (2016), 1–10.
- Marc Levoy and Pat Hanrahan. 1996. Light field rendering. In *Proceedings of the 23rd annual conference on Computer graphics and interactive techniques*. 31–42.
- Tianye Li, Mira Slavcheva, Michael Zollhoefer, Simon Green, Christoph Lassner, Changil Kim, Tanner Schmidt, Steven Lovegrove, Michael Goesele, and Zhaoyang Lv. 2021b. Neural 3d video synthesis. *arXiv preprint arXiv:2103.02597* (2021).
- Zhengqi Li, Simon Niklaus, Noah Snaveley, and Oliver Wang. 2021a. Neural scene flow fields for space-time view synthesis of dynamic scenes. In *Proceedings of the IEEE/CVF Conference on Computer Vision and Pattern Recognition*. 6498–6508.
- Lingjie Liu, Jiatao Gu, Kyaw Zaw Lin, Tat-Seng Chua, and Christian Theobalt. 2020. Neural sparse voxel fields. *arXiv preprint arXiv:2007.11571* (2020).
- Lingjie Liu, Marc Habermann, Viktor Rudnev, Kripasindhu Sarkar, Jiatao Gu, and Christian Theobalt. 2021. Neural Actor: Neural Free-view Synthesis of Human Actors with Pose Control. *arXiv preprint arXiv:2106.02019* (2021).
- Stephen Lombardi, Tomas Simon, Jason Saragih, Gabriel Schwartz, Andreas Lehrmann, and Yaser Sheikh. 2019. Neural volumes: Learning dynamic renderable volumes from images. *arXiv preprint arXiv:1906.07751* (2019).
- Stephen Lombardi, Tomas Simon, Gabriel Schwartz, Michael Zollhoefer, Yaser Sheikh, and Jason Saragih. 2021. Mixture of volumetric primitives for efficient neural rendering. *arXiv preprint arXiv:2103.01954* (2021).
- Ben Mildenhall, Pratul P Srinivasan, Rodrigo Ortiz-Cayon, Nima Khademi Kalantari, Ravi Ramamoorthi, Ren Ng, and Abhishek Kar. 2019. Local light field fusion: Practical view synthesis with prescriptive sampling guidelines. *ACM Transactions on Graphics (TOG)* 38, 4 (2019), 1–14.
- Ben Mildenhall, Pratul P Srinivasan, Matthew Tancik, Jonathan T Barron, Ravi Ramamoorthi, and Ren Ng. 2020. Nerf: Representing scenes as neural radiance fields for view synthesis. In *European conference on computer vision*. Springer, 405–421.
- Armin Mustafa, Hansung Kim, Jean-Yves Guillemaut, and Adrian Hilton. 2016. Temporally coherent 4d reconstruction of complex dynamic scenes. In *Proceedings of the IEEE Conference on Computer Vision and Pattern Recognition*. 4660–4669.
- Keunhong Park, Utkarsh Sinha, Jonathan T Barron, Sofien Bouaziz, Dan B Goldman, Steven M Seitz, and Ricardo Martin-Brualla. 2021a. Nerfies: Deformable neural radiance fields. In *Proceedings of the IEEE/CVF International Conference on Computer Vision*. 5865–5874.
- Keunhong Park, Utkarsh Sinha, Peter Hedman, Jonathan T Barron, Sofien Bouaziz, Dan B Goldman, Ricardo Martin-Brualla, and Steven M Seitz. 2021b. Hypernerf: A higher-dimensional representation for topologically varying neural radiance fields. *arXiv preprint arXiv:2106.13228* (2021).
- Sida Peng, Yuanqing Zhang, Yinghao Xu, Qianqian Wang, Qing Shuai, Hujun Bao, and Xiaowei Zhou. 2021. Neural body: Implicit neural representations with structured latent codes for novel view synthesis of dynamic humans. In *Proceedings of the IEEE/CVF Conference on Computer Vision and Pattern Recognition*. 9054–9063.
- Albert Pumarola, Enric Corona, Gerard Pons-Moll, and Francesc Moreno-Noguer. 2021. D-nerf: Neural radiance fields for dynamic scenes. In *Proceedings of the IEEE/CVF Conference on Computer Vision and Pattern Recognition*. 10318–10327.
- Nasim Rahaman, Aristide Baratin, Devansh Arpit, Felix Draxler, Min Lin, Fred Hamprecht, Yoshua Bengio, and Aaron Courville. 2019. On the spectral bias of neural networks. In *International Conference on Machine Learning*. PMLR, 5301–5310.
- Christian Reiser, Songyou Peng, Yiyi Liao, and Andreas Geiger. 2021. KiloNeRF: Speeding up Neural Radiance Fields with Thousands of Tiny MLPs. *arXiv preprint arXiv:2103.13744* (2021).
- Karen Simonyan and Andrew Zisserman. 2014. Very deep convolutional networks for large-scale image recognition. *arXiv preprint arXiv:1409.1556* (2014).
- Pratul P Srinivasan, Richard Tucker, Jonathan T Barron, Ravi Ramamoorthi, Ren Ng, and Noah Snaveley. 2019. Pushing the boundaries of view extrapolation with multiplane images. In *Proceedings of the IEEE/CVF Conference on Computer Vision and Pattern Recognition*. 175–184.
- Justus Thies, Michael Zollhöfer, and Matthias Nießner. 2019. Deferred neural rendering: Image synthesis using neural textures. *ACM Transactions on Graphics (TOG)* 38, 4 (2019), 1–12.
- Edgar Tretschk, Ayush Tewari, Vladislav Golyanik, Michael Zollhöfer, Christoph Lassner, and Christian Theobalt. 2021. Non-rigid neural radiance fields: Reconstruction and novel view synthesis of a dynamic scene from monocular video. In *Proceedings of the IEEE/CVF International Conference on Computer Vision*. 12959–12970.
- Dmitry Ulyanov, Vadim Lebedev, Andrea Vedaldi, and Victor S Lempitsky. 2016. Texture networks: Feed-forward synthesis of textures and stylized images.. In *ICML*, Vol. 1. 4.
- Minye Wu, Yuehao Wang, Qiang Hu, and Jingyi Yu. 2020. Multi-view neural human rendering. In *Proceedings of the IEEE/CVF Conference on Computer Vision and Pattern Recognition*. 1682–1691.
- Alex Yu, Sara Fridovich-Keil, Matthew Tancik, Qinhong Chen, Benjamin Recht, and Angjoo Kanazawa. 2021a. Plenoxels: Radiance Fields without Neural Networks. *arXiv preprint arXiv:2112.05131* (2021).
- Alex Yu, Ruilong Li, Matthew Tancik, Hao Li, Ren Ng, and Angjoo Kanazawa. 2021b. Plenotrees for real-time rendering of neural radiance fields. *arXiv preprint arXiv:2103.14024* (2021).
- Jiakai Zhang, Xinhang Liu, Xinyi Ye, Fuqiang Zhao, Yanshun Zhang, Minye Wu, Yingliang Zhang, Lan Xu, and Jingyi Yu. 2021. Editable free-viewpoint video using a layered neural representation. *ACM Transactions on Graphics (TOG)* 40, 4 (2021), 1–18.